Numerical Simulation of Flame Quenching and Acceleration by a Metal Foam

Hsiao-Chi Li and Ryan W. Houim
University of Florida
Gainesville, Florida, USA

1 Introduction

Reactive fuel-oxygen mixtures can be prone to unwanted combustion events and even detonation [1]. Flame arrestors are often placed in systems where explosion hazards may be a significant concern [2, 3]. Several flame arrestor concepts are based on open-cell metal foams that remove thermal energy from the flame and, if designed properly, quench reactions [4]. However, improperly-designed flame arrestors may exacerbate the unwanted ignition event. If length scales of the pores are too large, the struts of the foam may act as bluff bodies that promote turbulence, flame acceleration, and possible transition to detonation. Understanding how flames interact with metal foam structures can lead to improved safety designs, or be used to promote deflagration-to-detonation transition (DDT) if a detonation is wanted for applications such as propulsion [5]. Details of how flames interact with metal foams have not been extensively studied.

2 Problem Setup

In this work we present 3D numerical simulations of flame propagation through a metal foam structure by solving the fully compressible reactive Navier-Stokes equations. The solid surfaces representing the foam are embedded using an immersed boundary method (IBM) [6–8] with isothermal boundary conditions. The fuel-oxidizer mixture is stoichiometric hydrogen-oxygen at 300 K and 1 atm. Detailed chemical kinetics with 27 reactions and 8 species [9] and mixture-averaged transport are used.

The simulations cases consider in this paper are summarized in Table 1. Figure 1 shows the geometrical setup for the baseline geometry (Cases 1 and 5) presented in this paper. A metal foam structure is placed inside of a square channel to interact with a propagating stoichiometric H_2-O_2 flame. The baseline case considers a channel of length 16 mm with a 1 mm by 1 mm square cross-section. The influence of channel size is explored by multiplying all dimensions of the channel and foam by a scaling factor to produce geometrically similar channels. Two initial condition configurations are considered. The first is a planar flame that is ignited by constant-pressure equilibrium products of stoichiometric H_2-O_2. The high-temperature products are located at a distance of 4 mm from the left-end of the domain for the baseline geometry. The second configuration considers a flame ignited by a spherical spark that is 400 μm in diameter at $10,000$ K and 100 atm. The spark diameter is not scaled with the channel size.

Correspondence to: rhouim@ufl.edu

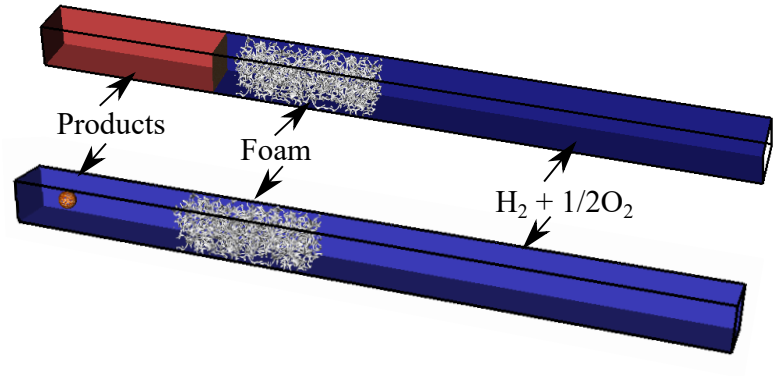

Figure 1: Initial conditions showing (top) the planar and (bottom) spherical flame initial conditions for a stoichiometric H_2 and O_2 flame propagating in a closed channel with a metal foam inserted. The boundary conditions on the sides and right end are symmetry planes channel. The left boundary condition is a non-reflecting outflow.

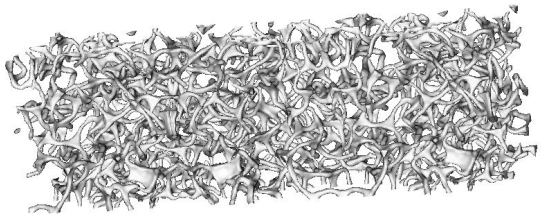

Figure 2: The foam geometry used in the simulation.

Figure 2 shows a closeup view of the metal foam embedded in the computational domain. The stereolithography (STL) file for the metal foam was obtained from https://grabcad.com/library/auxetic-foam-sample-1. The length of the foam is 2.5 mm and the left end is placed 4.5 mm from the left boundary for baseline channel size (Cases 1 and 5). The dimensions of the foam are scaled along with the channel size for other five cases. Isothermal and no-slip boundary conditions at 300 K are used on the embedded foam. The foam is inserted into the domain using an advanced immersed boundary method (IBM) [7, 10, 11]. A ghost-fluid method is used to enforce boundary conditions on the foam [6, 7].

The governing equation were solved using an operator splitting approach. The hydrodynamic terms where computed using a high-order Godunov method with seventh-order WENO and the HLLC flux for spatial discretization of the hyperbolic terms. Second-order central differencing was used for the viscous and diffusion terms [12]. The yet-another-stiff-solver (YASS) [13] was used to integrate the chemical source terms. Adaptive mesh refinement was implemented using the massively-parallel AMReX library [14]. The simulations used two levels of refinement with 128 cells across the channel at the finest level. This corresponds to a grid spacing of 7.8 μm which is $\sim$ 31 cells in the thermal thickness of a laminar H_2-O_2 flame for the baseline channel size. The numerical code, HyBurn, used in this work has been extensively verified and validated for scenarios including laminar flames, detonations, a variety of Riemann problems, and shock-obstacle interactions.

3 Results

Figure 3 shows time sequence plots for Cases 4 and 7. In Case 7 (spherical spark ignition with a channel height of 4 mm) the small flame kernel elongates due to preferential flow along the channel axis and

Table 1: List of simulation cases and results.

Case	Initial Flame	Channel Height (mm)	Result
1	Planar	1 by 1	quench
2	Planar	1.1	shock and flame
3	Planar	1.5	detonation
4	Planar	2	detonation
5	Spherical	1	quench
6	Spherical	2	shock and flame
7	Spherical	4	shock and flame

also interactions with weak shock reflections produced by the high pressure in the spark. At 206 μs, the flame kernel grows close to the side walls and also enters the foam. The flame accelerates as it propagates through the tortuous path created by foam struts. The flame exits the foam about 20 μs later and with an averaged flame velocity of $\sim$ 600 m/s inside of the foam. The resulting shock and turbulent flame complex [1] propagates downstream of the foam.

The results for Case 4 show a scenario where the planar flame grows and propagates into the foam. The flame reaches the foam at $\sim$ 71 μs and exits the foam at $\sim$ 88 μs. Unlike Case 7, a detonation is initiated as the flame exits the foam. The exact mechanism of detonation initiation by the foam are currently being analyzed.

Figure 4 shows a time series of temperature slices at the centerline of the channel for Cases 1 and 4 (planar ignition). The flame enters the foam at 24 μs for Case 1 (1 mm-high channel). The heat loss from the reaction zone of the flame due to the foam is too high and ultimately quenches the combustion wave. As already discussed above, the flame enters the foam for Case 4 (2 mm-high channel) at about 71 μs and rapidly accelerates. A detonation emerges from the foam and continues to propagate downstream. Similar to Case 4, the flame propagates through the foam and transitions to detonation in Case 3 as shown in Fig. 5.

Cases 1 and 4 illustrate the extreme limits of how the foam can interact with the flame in ways can either quench the reaction or promote DDT. Case 2 (1.1 mm-high channel), shown in Fig. 5, represents a scenario between these two extreme limits. In Case 2, the flame enters the foam at $\sim$ 90 μs and continues to propagate. However, in this case, the heat losses and shorter length of the foam do not accelerate the flame to the point where a detonation is initiated. Instead, the flame exits the foam as a decoupled turbulent shock-flame complex [1].

Figure 6 shows temperature slices for Cases 6 and 7 which consider the high-temperature and high-pressure spark initial conditions. The initial dynamics of the flame are significantly different than they are for the planar ignition scenario (Cases 1-4). Here, the small 400 μm-diameter flame kernel growths and the high initial pressure in the spark produces weak shocks waves. These weak shocks reflect from the channel walls to produce complex-shaped flame shapes observed at 35 μs for Case 6. The flame grows and expands in the flow produced by these weak shocks. The flame interacts with the foam at $\sim$ 59 μs for Case 6 and emerges $\sim$ 20 μs later as a turbulent shock-flame complex. Separate ignition kernels form in front of the main turbulent flame at $\sim$ 95 μs, but do not initiate a detonation. The results for Case 7 are similar to Case 6. However, there are some differences in timing due to the increased distance between the spark location and the foam. The flame is quenched by the foam for Case 5, which is not shown.

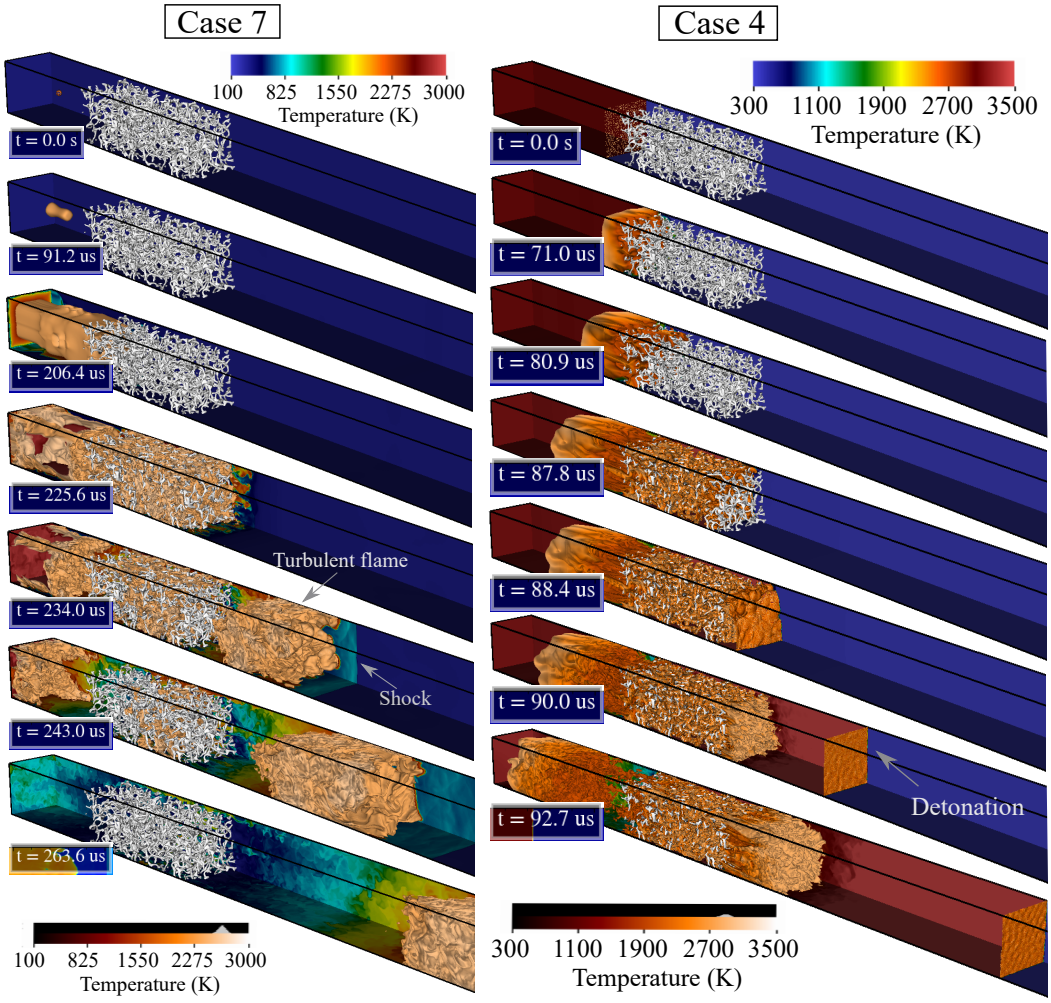

Figure 3: Computed results for (left) Case 7 and (right) Case 4 showing a time series of volume renderings of temperature and the embedded foam. Slices of temperature are shown on the left, bottom, and rear walls of the domain.

4 Discussion and Conclusions

The results shown in this work indicate that open-cell metal foams can significantly alter the dynamics of propagating flames by either quenching them or promoting flame acceleration. In extreme cases the flame accelerates rapidly and undergoes DDT. The results indicate that the effect of the foam on the flame is a competition between convective heat loss trying to quench the flame and hydrodynamic effects induced by the foam struts trying to accelerate the flame. The foam struts behave similarly to obstacles in channels that induce turbulence and shock reflections which are well-known to promote flame acceleration and even initiate detonation [1]. The flame quenches in Cases 1 and 5 due to heat losses from the reaction zone of the flame by the foam. Cases 2, 6, and 7 have larger pore structures which accelerated the flame due to gas-dynamic effects introduced by the flow interacting with the foam struts. In addition to these gas dynamic effects, mean hydraulic resistance introduced by the foam may also induce pressure gradients that may also alter the dynamics of the flame.

Our ongoing work is exploring the detailed physical mechanisms of flame quenching, acceleration, and transition to detonation by metal foam structures. Scenarios where the foam length is constant will be considered and quantitative analysis on the competition between chemical energy release and heat-loss

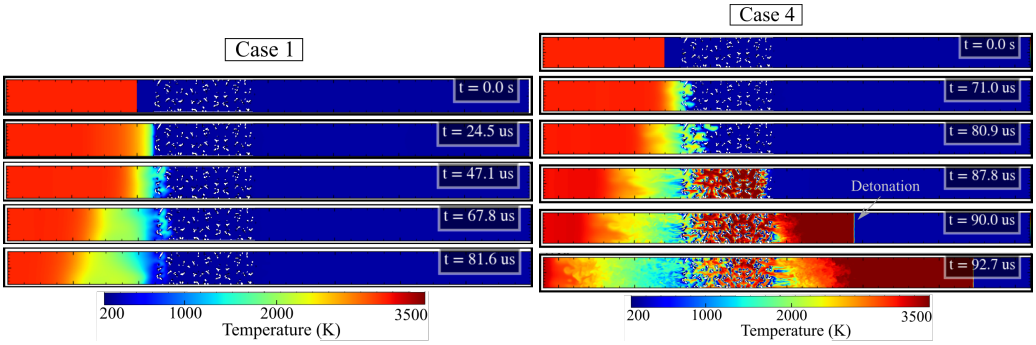

Figure 4: Time series showing temperature slices for (left) Case 1 and (right) Case 4. The slices are generated at the center plane of the channel.

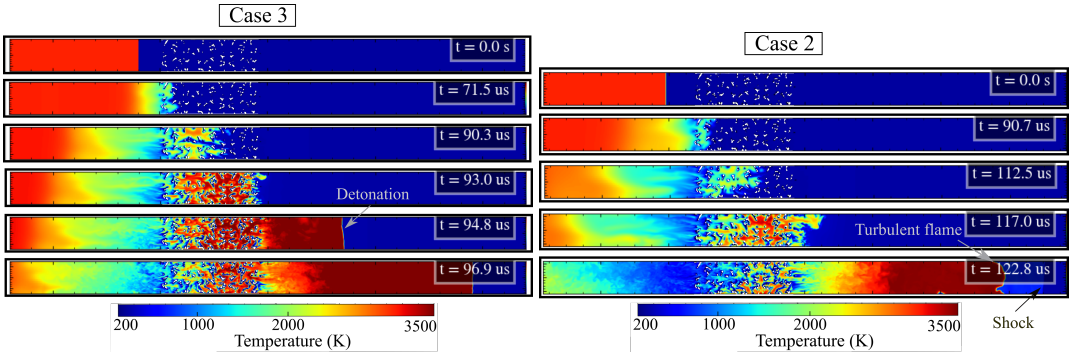

Figure 5: Time series showing temperature slices for (left) Case 3 and (right) Case 2. The slices are generated at the center plane of the channel.

rates will be analyzed.

5 Acknowledgements

This work was supported in part by Air Force Office of Scientific Research grant FA9550-19-1-0023, Naval Research Laboratory contract N00173-18-P-0352, and National Science Foundation grant 1942861.

References

[1] Oran, E. S. and Gamezo, V. N., "Origins of the deflagration-to-detonation transition in gas-phase combustion," *Combustion and Flame*, Vol. 148, No. 1-2, 2007, pp. 4–47.

[2] Kakutkina, N., Korzhavin, A., and Rychkov, A., "Burning-through of porous flame arresters with a channel flame-arrester element," *Combustion, Explosion, and Shock Waves*, Vol. 45, No. 3, 2009, pp. 266–273.

[3] AL-Zuraiji, M. J. A., Zanganeh, J., and Moghtaderi, B., "Application of flame arrester in mitigation of explosion and flame deflagration of ventilation air methane," *Fuel*, Vol. 257, 2019, pp. 115985.

[4] Chen, P., Huang, F., Sun, Y., and Chen, X., "Effects of metal foam meshes on premixed methane-air flame propagation in the closed duct," *Journal of Loss Prevention in the Process Industries*, Vol. 47, 2017, pp. 22–28.

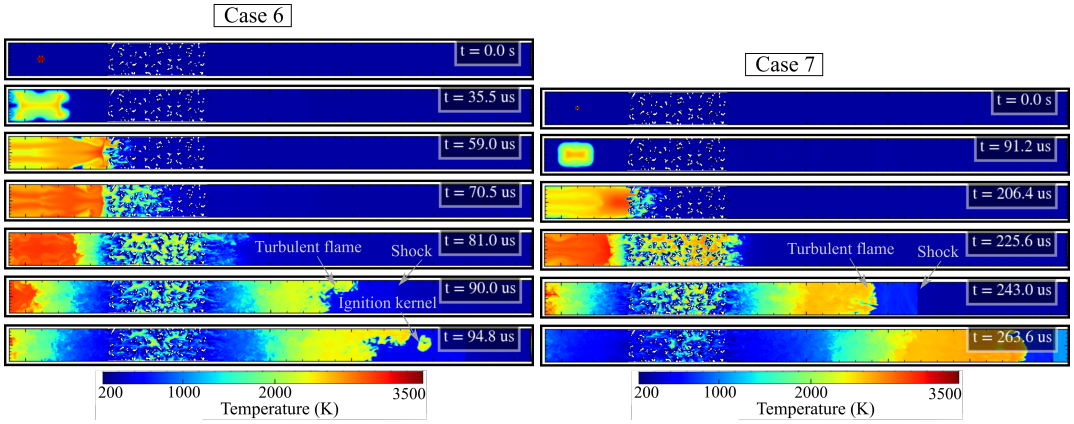

Figure 6: Time series showing temperature slices as the flame interacts with the metal foam for (left) Case 6 and (right) Case 7. The slices are taken at the center plane of the channel.

[5] Wolański, P., "Detonative propulsion," *Proceedings of the combustion Institute*, Vol. 34, No. 1, 2013, pp. 125–158.

[6] Chaudhuri, A., Hadjadj, A., and Chinnayya, A., "On the use of immersed boundary methods for shock/obstacle interactions," *Journal of Computational Physics*, Vol. 230, No. 5, 2011, pp. 1731–1748.

[7] Mo, H., Lien, F.-S., Zhang, F., and Cronin, D. S., "An immersed boundary method for solving compressible flow with arbitrarily irregular and moving geometry," *International Journal for Numerical Methods in Fluids*, Vol. 88, No. 5, 2018, pp. 239–263.

[8] Peskin, C. S., "The immersed boundary method," *Acta numerica*, Vol. 11, 2002, pp. 479–517.

[9] Burke, M. P., Chaos, M., Ju, Y., Dryer, F. L., and Klippenstein, S. J., "Comprehensive H2/O2 kinetic model for high-pressure combustion," *International Journal of Chemical Kinetics*, Vol. 44, No. 7, 2012, pp. 444–474.

[10] Mittal, R. and Iaccarino, G., "Immersed boundary methods," *Annu. Rev. Fluid Mech.*, Vol. 37, 2005, pp. 239–261.

[11] Li, H.-C. and Houim, R. W., "A fast algorithm for embedding complex geometry into block-structured adaptive mesh refiment codes," *Computers and Fluids*, 2021, Under Review.

[12] Houim, R. W. and Kuo, K. K., "A low-dissipation and time-accurate method for compressible multi-component flow with variable specific heat ratios," *Journal of Computational Physics*, Vol. 230, No. 23, 2011, pp. 8527–8553.

[13] Khokhlov, A., Austin, J., and Bacon, C., "First-Principles Petascale Simulations for Predicting Deflagration to Detonation Transition in Hydrogen-Oxygen Mixtures," Tech. rep., Univ. of Chicago, IL (United States), 2015.

[14] Zhang, W., Almgren, A., Beckner, V., Bell, J., Blaschke, J., Chan, C., Day, M., Friesen, B., Gott, K., Graves, D., Katz, M., Myers, A., Nguyen, T., Nonaka, A., Rosso, M., Williams, S., and Zingale, M., "AMReX: a framework for block-structured adaptive mesh refinement," *Journal of Open Source Software*, Vol. 4, No. 37, May 2019, pp. 1370.